Molecular Motions in Highly Disordered Solid Phases of $[(CH_3)_3NCH_2CH_3]X$ ($X = ClO_4$, PF_6, NO_3) Studied by ^1H, ^{19}F, and ^{14}N NMR, Powder X-Ray Diffraction, and Differential Scanning Calorimetry

Hiroshi Ono, Shin'ichi Ishimaru, Ryuichi Ikeda, and Hiroyuki Ishida[*,†]

Department of Chemistry, University of Tsukuba, Tsukuba 305

†Department of Chemistry, Faculty of Science, Okayama University, Okayama 700

(Received June 18, 1997)

^1H, ^{19}F, and ^{14}N NMR, powder X-ray diffraction, and differential scanning calorimetry (DSC) were measured in trimethylethylammonium perchlorate, hexafluorophosphate and nitrate, $[(CH_3)_3NCH_2CH_3]X$ ($X = ClO_4$, PF_6, NO_3). Three, four and four solid phases were obtained for perchlorate, hexafluorophosphate, and nitrate, respectively, in the temperature ranges from 77 K to their decomposition temperatures. X-Ray powder patterns showed that the highest-temperature solid phases of perchlorate and hexafluorophosphate are CsCl-type cubic, while that of nitrate is NaCl-type cubic. The second highest-temperature phases of perchlorate and hexafluorophosphate form tetragonal lattices. The NMR study revealed that the cations perform isotropic rotation as well as self-diffusion in the CsCl-type cubic and tetragonal phases of perchlorate. In the cubic phase of hexafluorophosphate, isotropic rotation and self-diffusion of both anion and cation were observed. In the NaCl-type cubic phase of nitrate, isotropic rotation of both ions was detected. The structures in the highest- and second highest-temperature phases of the three salts were found to be dynamically disordered. Especially, the highest-temperature phases of perchlorate and hexafluorophosphate can be classified into the ionic plastic phase of the CsCl-type structure. Activation energies of the ionic motions in these phases were evaluated. Motional modes of the ions in the lower temperature phases were also deduced.

In the previous papers, we studied $[(CH_3)_3NCH_2CH_3]I$[1] and $[(CH_3)_3NCH_2CH_3]BF_4$[2] by ^1H, ^{127}I, ^{19}F, and ^{14}N NMR, powder X-ray diffraction, and thermal measurements. We found that iodide and tetrafluoroborate have three and five solid phases, respectively, above 77 K and we discussed disordered ionic orientations formed in high-temperature phases. Especially, the highest-temperature solid phases of these salts are highly-disordered and crystallize in the NaCl-type cubic structure, where $(CH_3)_3NC_2H_5^+$ and BF_4^- ions perform isotropic rotation. Moreover, self-diffusion of I^- and BF_4^- ions was observed in these phases. Self-diffusion of the bulky cation, however, was not detected in the NMR time scale. These phases can be regarded as one of mesophases characteristic of ionic crystals,[3,4] in which the degree of motional freedom of ions is comparable with that of molecules in the plastic crystal.[5,6]

In the present investigation, we have studied three kinds of salts $[(CH_3)_3NCH_2CH_3]X$ ($X = ClO_4$, PF_6, NO_3), in order to reveal the solid–solid phase transitions and the presence of the mesophase similar to that in iodide and tetrafluoroborate.

Experimental

$[(CH_3)_3NC_2H_5]ClO_4$ and $[(CH_3)_3NC_2H_5]PF_6$ were prepared by neutralizing trimethylethylammonium hydroxide with respective acids. Trimethylethylammonium hydroxide was prepared from $[(CH_3)_3NC_2H_5]I$ (purchased from Tokyo Kasei) using the anion exchange resin (DOWEX 1X-8, Dow Chemical). $[(CH_3)_3NC_2H_5]NO_3$ was directly obtained from iodide by use of the anion exchange resin. The obtained crystals of $[(CH_3)_3NC_2H_5]ClO_4$ and $[(CH_3)_3NC_2H_5]NO_3$ were recrystallized twice from methanol and ethanol, respectively. $[(CH_3)_3NC_2H_5]PF_6$ was recrystallized twice by cooling the aqueous solution from ca. 80 °C to room temperature. Found: C, 32.16; H, 7.51; N, 7.49%. Calcd for $[(CH_3)_3NC_2H_5]ClO_4$: C, 32.01; H, 7.52; N, 7.47%. Found: C, 25.88; H, 6.09; N, 5.92%. Calcd for $[(CH_3)_3NC_2H_5]PF_6$: C, 25.76; H, 6.05; N, 6.01%. Found: C, 39.40; H, 9.37; N, 18.32%. Calcd for $[(CH_3)_3NC_2H_5]NO_3$: C, 39.98; H, 9.40; N, 18.66%. The purified crystals were dried under vacuum (ca. 10^{-1} Pa) at room temperature for 24 h before measurements of NMR and DSC.

Phase transition temperatures and corresponding enthalpy changes were determined by a Seiko Instruments DSC 120 calorimeter. Powder X-ray patterns were taken by using a Philips X'pert PW3040/00 diffractometer. The second moment of ^1H and ^{19}F NMR linewidth was measured using a Bruker SXP100 spectrometer by employing the solid-echo method.[7] Spin-lattice relaxation times (T_1) and spin–spin relaxation times (T_2) of ^1H and ^{19}F NMR were measured by use of a homemade pulse NMR spectrometer[8] and the SXP100 spectrometer. The $180°-\tau-90°$ pulse sequence and the Hahn's spin-echo method[9] were employed for the determination of T_1 and T_2, respectively. ^{14}N NMR spectra were obtained on a Bruker MSL300 spectrometer at a Larmor frequency of 21.67 MHz using the quadrupole-echo method.[10] As the standard of the chemical shift of ^{14}N NMR, we used a 10% nitric acid having a chemical shift of −5.6 ppm from neat nitromethane.

Results

Differential Scanning Calorimetry (DSC) and X-Ray Diffraction. DSC was measured in the temperature range from 150 to 630 K. Three, four and four solid phases were observed in $[(CH_3)_3NC_2H_5]X$ (X = ClO_4, PF_6, and NO_3), respectively. The obtained solid phases are designated as Phases I, II, III, and IV in the order of decreasing temperature. Transition temperatures (T_{tr}), corresponding enthalpy changes ($\Delta_{tr}H$) and entropy changes ($\Delta_{tr}S$) are summarized in Table 1. Data on $[(CH_3)_3NC_2H_5]X$ (X = I, BF_4)[1,2] are included for comparison.

The powder X-ray diffraction angles (2θ) in Phases I and II of $[(CH_3)_3NC_2H_5]ClO_4$ taken at ca. 450 and 300 K, respectively, are shown in Table 2. The structure of Phase I could be well interpreted by a CsCl-type cubic lattice with $a=6.28(2)$ Å, $Z=1$, $V=248(3)$ Å^3, and $D_X=1.26(1)$ Mg m^{-3}, and that of Phase II by a tetragonal lattice with $a=8.67(2)$, $c=6.30(2)$ Å, $Z=2$, $V=473(4)$ Å^3, and $D_X=1.32(1)$ Mg m^{-3}. Table 3 shows the X-ray data in Phases I and II of $[(CH_3)_3NC_2H_5]PF_6$ obtained at ca. 400 and 300 K, respectively. The data of Phase I were assigned to a CsCl-type cubic lattice with $a=6.43(2)$ Å, $Z=1$, $V=265(3)$ Å^3, and $D_X=1.46(2)$ Mg m^{-3}, and that of Phase II to a tetragonal lattice with $a=8.94(2)$, $c=6.42(3)$ Å, $Z=2$, $V=513(5)$ Å^3, and $D_X=1.51(1)$ Mg m^{-3}. The Phases II of perchlorate and hexafluorophosphate are expected to be isomorphous from the obtained patterns. Table 4 shows the X-ray data in Phase I of $[(CH_3)_3NC_2H_5]NO_3$ taken at ca. 400

Table 2. Observed and Calculated 2θ Values of X-Ray Powder Patterns of $[(CH_3)_3NC_2H_5]ClO_4$ Taken at ca. 450 K in Phase I and at ca. 300 K in Phase II. (Phase I: cubic, $a=6.28(2)$ Å, $Z=1$; Phase II: tetragonal, $a=8.67(2)$, $c=6.30(2)$ Å, $Z=2$; λ (Cu $K\alpha_1$) = 1.54060 Å)

Observed		Calculated	
2θ (deg)	I (%)	2θ (deg)	*hkl*
Phase I			
14.10	5	14.09	100
20.00	100	19.98	110
24.51	3	24.53	111
28.39	5	28.40	200
31.86	4	31.83	210
34.94	2	34.96	211
Phase II			
14.12	1	14.04	001
14.46	6	14.45	110
17.38	30	17.39	101
20.20	100	20.20	111
20.50	60	20.49	200
24.93	2	24.93	201
27.01	30	27.00	211
29.13	5	29.14	220
30.16	12	30.16	102
32.56	1	32.47	221
32.67	5	32.67	310
34.18	1	34.12	301
35.72	2	35.72	311

Table 1. Transition Temperatures (T_{tr}), Enthalpy Changes ($\Delta_{tr}H$), and Entropy Changes ($\Delta_{tr}S$) Determined by Differential Scanning Calorimetry (DSC) for solid $[(CH_3)_3NC_2H_5]$-X (X = ClO_4, PF_6, NO_3, I, BF_4)

Compound	T_{tr} (K)	$\Delta_{tr}H$ (kJ mol^{-1})	$\Delta_{tr}S$ (J K^{-1} mol^{-1})
$[(CH_3)_3NC_2H_5]ClO_4$	259	11±1	42±1
	432	0.44±0.12	1.0±0.4
	603	Decomposed	
$[(CH_3)_3NC_2H_5]PF_6$	197	1.8±0.1	9.1±0.1
	247	0.72±0.05	2.9±0.1
	343	0.26±0.03	0.75±0.06
	637	Decomposed	
$[(CH_3)_3NC_2H_5]NO_3$	209	0.42±0.16	2.0±0.8
	243	6.6±0.1	27±1
	332	7.9±0.1	24±1
	547	Decomposed	
$[(CH_3)_3NC_2H_5]I$[a]	336	6.23±0.06	18.5±0.2
	410	8.81±0.06	21.5±0.2
	ca. 530	ca. 2.0 (mp with decomposition)	ca. 5.5
$[(CH_3)_3NC_2H_5]BF_4$[b]	222	0.16±0.05	0.7±0.2
	239	1.80±0.05	7.5±0.2
	293	2.1±0.1	7.2±0.4
	362	4.5±0.1	12.4±0.3
	630	Decomposed	

a) Ref. 1. b) Ref. 2.

Table 3. Observed and Calculated 2θ Values of X-Ray Powder Patterns of $[(CH_3)_3NC_2H_5]PF_6$ Taken at ca. 400 K in Phase I and at ca. 300 K in Phase II (Phase I: cubic, $a=6.43(2)$ Å, $Z=1$; Phase II: tetragonal, $a=8.94(3)$, $c=6.42(3)$ Å, $Z=2$; λ (Cu $K\alpha_1$) = 1.54060 Å)

Observed		Calculated	
2θ (deg)	I (%)	2θ (deg)	hkl
Phase I			
13.81	10	13.77	100
19.56	100	19.52	110
23.99	1	23.97	111
27.76	5	27.74	200
31.06	1	31.10	210
Phase II			
13.82	5	13.81	001
14.06	20	14.02	110
17.06	10	17.02	101
19.74	100	19.37	111
19.91	60	19.88	200
24.28	1	24.28	201
26.27	10	26.28	211
28.26	5	28.26	220
29.59	5	29.60	102
31.57	1	31.58	221
31.69	1	31.63	310
33.16	1	33.17	301

Table 4. Observed and Calculated 2θ Values of X-Ray Powder Patterns in Phase I of $[(CH_3)_3NC_2H_5]NO_3$ Taken at ca. 400 K (cubic, $a=9.83(2)$ Å, $Z=4$, λ (Cu $K\alpha_1$ = 1.54060 Å)

Observed		Calculated	
2θ (deg)	I (%)	2θ (deg)	hkl
15.59	1	15.60	111
18.00	100	18.03	200
25.65	18	25.61	220
30.13	4	30.13	311
31.50	3	31.50	222

K. They were explained by an NaCl-type cubic lattice with $a=9.83(2)$, $Z=4$, $V=950(6)$ Å^3 and $D_X=1.05(1)$ Mg m^{-3}. The powder pattern in Phase II taken at ca. 300 K was explicable in terms of neither cubic nor tetragonal lattice, implying a lower crystal symmetry. The structural data are summarized in Table 5 together with those of $[(CH_3)_3NC_2H_5]X$ (X = I, BF_4).[1,2]

NMR: (1) $[(CH_3)_3NC_2H_5]ClO_4$. The temperature dependence of second moment (M_{2H}) of ^{1}H NMR linewidth in $[(CH_3)_3NC_2H_5]ClO_4$ observed at a Larmor frequency of 39.8 MHz is shown in Fig. 1. M_{2H} in Phase III has a constant value of $(17.8\pm0.5)\times10^{-2}$ mT^2 in the range of 150—210 K. At the transition temperature from Phase III to II, abbreviated to T_{tr}(III→II), a discontinuous change in M_{2H} was observed. M_{2H} has a constant value of $(1.4\pm0.3)\times10^{-2}$ mT^2 between 260 and 390 K in Phase II. Above 390 K M_{2H}

Table 5. Structural Data of $[(CH_3)_3NC_2H_5]X$ (X = ClO_4, PF_6, NO_3, I, BF_4)

Compound	Temperature	Crystal system	Lattice	V	Z	D_X	Temperature
Phase	range (K)		Å	Å^3		Mg m^{-3}	K
$[(CH_3)_3NC_2H_5]ClO_4$							
Phase I	432—603	Cubic (CsCl-type)	$a=6.28(2)$	248(3)	1	1.26(1)	450
Phase II	259—432	Tetragonal	$a=8.67(2)$	473(4)	2	1.32(1)	300
			$c=6.30(2)$				
$[(CH_3)_3NC_2H_5]PF_6$							
Phase I	343—637	Cubic (CsCl-type)	$a=6.43(2)$	265(3)	1	1.46(2)	400
Phase II	247—343	Tetragonal	$a=8.94(2)$	513(5)	2	1.51(1)	300
			$c=6.42(3)$				
$[(CH_3)_3NC_2H_5]NO_3$							
Phase I	332—547	Cubic (NaCl-type)	$a=9.83(2)$	950(6)	4	1.05(1)	400
$[(CH_3)_3NC_2H_5]I$[a]							
Phase I	410—530	Cubic (NaCl-type)	$a=10.00(1)$	1000(3)	4	1.429(5)	430
Phase II	336—410	Tetragonal	$a=8.430(5)$	442(2)	2	1.617(8)	360
			$c=6.216(4)$				
Phase III	—336	Orthorhombic	$a=11.294(4)$	867(1)	4	1.647(2)	300
		(*Pnam*)	$b=10.729(2)$				
			$c=7.158(6)$				
$[(CH_3)_3NC_2H_5]BF_4$[b]							
Phase I	362—630	Cubic (NaCl-type)	$a=10.14(2)$	1043(3)	4	1.114(3)	400
Phase II	293—362	Tetragonal	$a=8.59(2)$	460(2)	2	1.26(2)	300
			$c=6.24(2)$				

a) Ref. 1. b) Ref. 2.

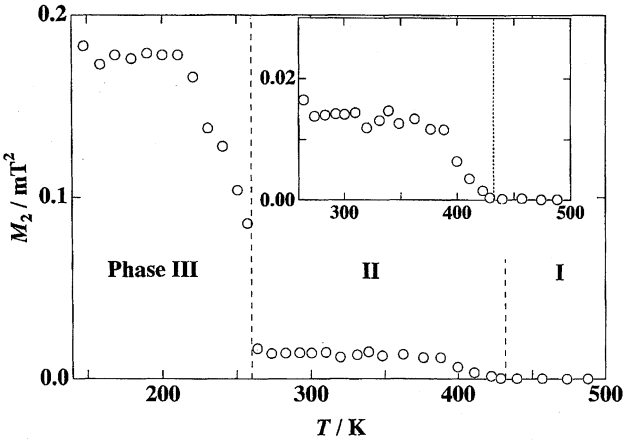

Fig. 1. The temperature dependence of second moment (M_2) of ^{1}H NMR linewidth observed in $[(CH_3)_3NC_2H_5]ClO_4$. The broken lines show the phase transition temperatures determined by DSC.

decreased with increasing temperature and became less than 0.05×10^{-2} mT^2 above 430 K in Phases II and I.

The temperature variation of ^{14}N NMR spectra observed from 300 K in Phase II to 435 K in Phase I is shown in Fig. 2. The quadrupole coupling constant (e^2Qqh^{-1}) and the asymmetry parameter (η) of the spectrum at 300 K were evaluated to be 8.1±0.2 kHz and less than 0.1, respectively. The spectrum became narrow, keeping its structure with increasing temperature in Phase II. On going from Phase II to I the structure disappeared while a single peak with a half-height width of 68±4 Hz appeared.

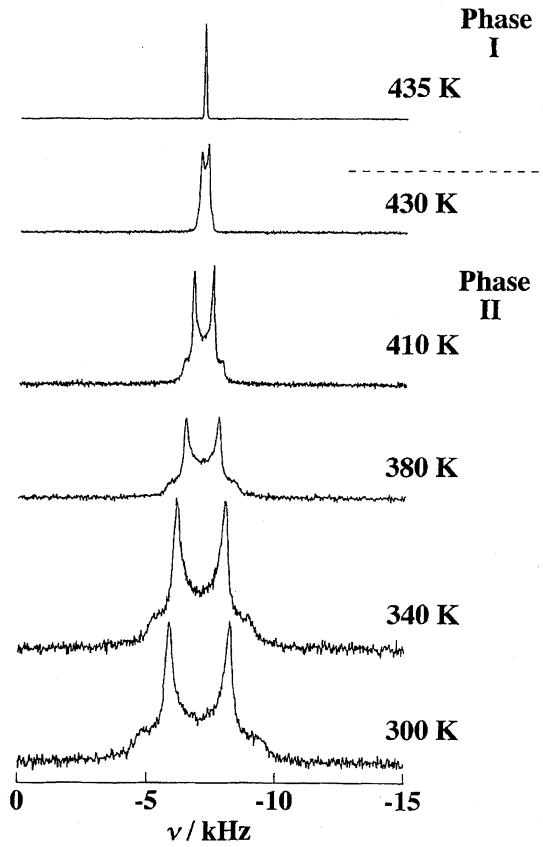

Fig. 2. The temperature variation of ^{14}N NMR spectra observed in Phases I and II of $[(CH_3)_3NC_2H_5]ClO_4$.

The temperature dependence of T_1 of ^{1}H NMR (abbreviated to T_{1H}) determined between 100 and 500 K at a Larmor frequency of 33.4 MHz is shown in Fig. 3. Two T_{1H} minima of 40 and 60 ms were obtained at ca. 165 and 240 K, respectively, in Phase III. T_{1H} at 62.9, 33.4, and 12.8 MHz and T_2 of ^{1}H NMR (abbreviated to T_{2H}) determined at 39.8 MHz in Phases II and I are shown in Fig. 4. T_{1H} in Phase II increased with increasing temperature and was independent of the Larmor frequency employed. T_{1H} in Phase I had a maximum value and was frequency dependent. T_{2H} increased from 80 μs on heating above 400 K in Phase II and reached to 15 ms at 500 K in Phase I.

(2) $[(CH_3)_3NC_2H_5]PF_6$. The temperature dependences of M_{2H} and the second moment (M_{2F}) of ^{19}F NMR linewidth determined at 40.9 and 38.6 MHz, respectively, are shown in Fig. 5. M_{2H} was 42.1×10^{-2} mT^2 at 173 K in Phase IV and decreased with increasing temperature. Almost constant M_{2H} values of $(8.5\pm1.0)\times10^{-2}$ and $(1.5\pm0.3)\times10^{-2}$ mT^2 were obtained in Phases III and II, respectively. On the other hand, M_{2F} had two plateau values of $(3.0\pm1.0)\times10^{-2}$ mT^2 in Phase IV and $(2.2\pm0.6)\times10^{-2}$ mT^2 in Phases III and II. In Phase I, both M_{2H} and M_{2F} decreased with increasing temperature and became less than 0.05×10^{-2} mT^2 above 485 K.

The ^{14}N NMR spectra observed in Phases I and II are shown in Fig. 6. The spectra showed a single peak whose half-height width decreased from 910±20 to 60±5 Hz with increasing temperature from 300 to 490 K. No discontinuous change in the linewidth was observed at T_{tr}(II→I).

The temperature variations of T_{1H} and T_1 of ^{19}F NMR (abbreviated to T_{1F}) determined at 36.1 and 34.0 MHz, respectively, in the temperature range from 90 to 490 K are shown in Fig. 7. Below 110 K in Phase IV, T_{1H} and T_{1F}

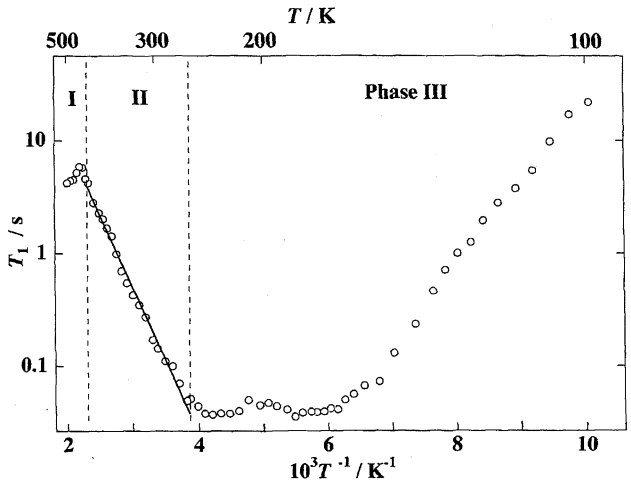

Fig. 3. The temperature dependence of ^{1}H NMR spin-lattice relaxation time (T_{1H}) of $[(CH_3)_3NC_2H_5]ClO_4$ observed at 33.4 MHz. The solid line shows the best-fitted theoretical values. The broken lines show the phase transition temperatures determined by DSC.

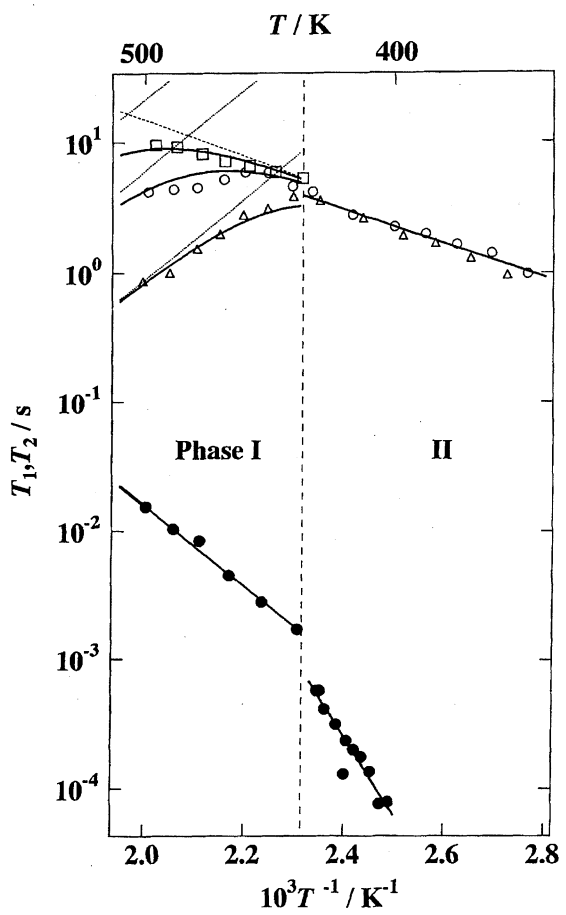

Fig. 4. Temperature dependences of ^{1}H NMR spin–lattice relaxation time (T_{1H}) and spin–spin relaxation time (T_{2H}) of $[(CH_3)_3NC_2H_5]ClO_4$. T_{1H} (□) observed at 62.9 MHz; T_{1H} (○) at 33.4 MHz; T_{1H} (△) at 12.8 MHz; T_{2H} (●) at 39.8 MHz. Solid and dotted lines are the best-fitted calculated values. The broken line shows the phase transition temperature determined by DSC.

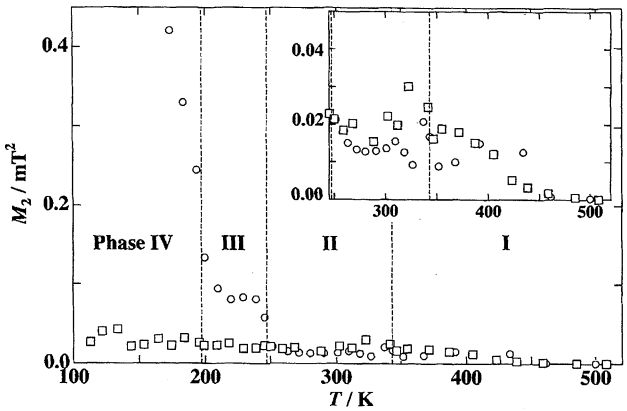

Fig. 5. Temperature dependences of second moments (M_2) of ^{1}H (○) and ^{19}F (□) NMR absorptions observed in $[(CH_3)_3NC_2H_5]PF_6$. The broken lines show the phase transition temperatures determined by DSC.

showed marked non-exponential recovery of the magnetization, which could be separated into two relaxation times, T_1^s and T_1^l ($T_1^s < T_1^l$), according to the following equation:

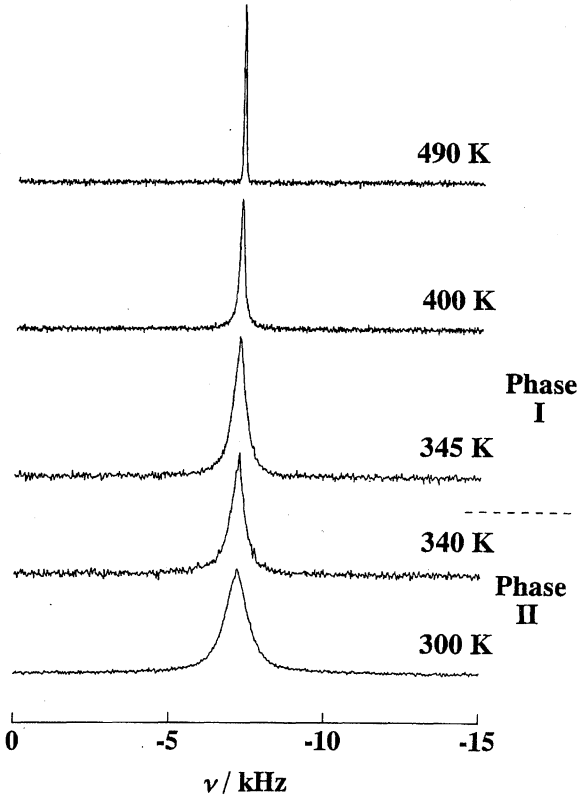

Fig. 6. The temperature variation of ^{14}N NMR spectra observed in Phases I and II of $[(CH_3)_3NC_2H_5]PF_6$.

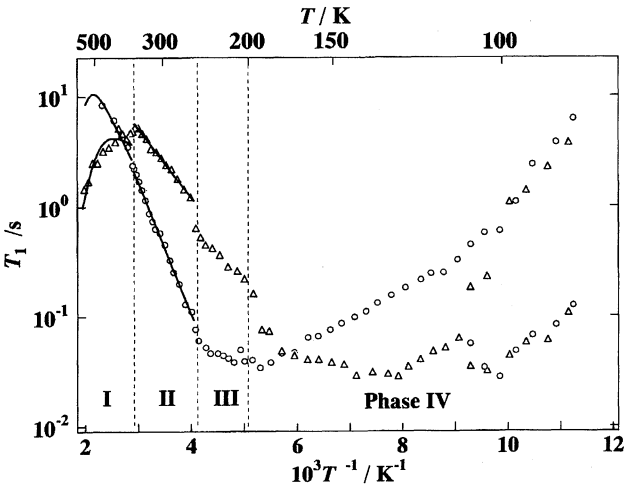

Fig. 7. Temperature dependences of spin-lattice relaxation times ^{1}H (T_{1H}) (○) and ^{19}F (T_{1F}) (△) in $[(CH_3)_3NC_2H_5]PF_6$ observed at 36.1 and 34.0 MHz, respectively. Solid lines are the best-fitted calculated values. The broken lines show the phase transition temperatures determined by DSC.

$$(M_0 - M_z(t))/2M_0 = A_s \exp(-t/T_1^s) + A_l \exp(-t/T_1^l). \quad (1)$$

Here, M_0 and $M_Z(t)$ are z-components of the ^{1}H or ^{19}F magnetization at thermal equilibrium and at time t after a 180° pulse, respectively, and A_s and A_l are constants ($A_s + A_l = 1$). A T_{1H} minimum was obtained around 200 K and two T_{1F} minima at ca. 100 and 140 K. Figure 8 shows the data of T_{1H} determined at 36.1 and 13.8 MHz, T_{1F} at 34.0 MHz, T_{2H}

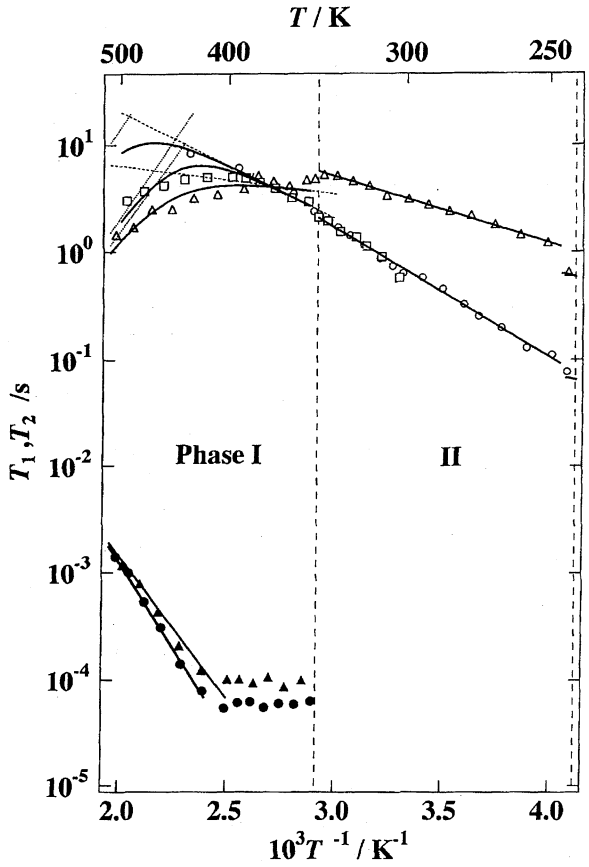

Fig. 8. Temperature dependences of spin–lattice relaxation time for ^1H (T_{1H}) and ^{19}F (T_{1F}), and spin–spin relaxation time for ^1H (T_{2H}) and ^{19}F (T_{2F}) observed in $[(CH_3)_3NC_2H_5]PF_6$. T_{1H} (○) at 36.1 MHz; T_{1H} (□) at 13.8 MHz; T_{1F} (△) at 34.0 MHz; T_{2H} (●) at 26.9 MHz; T_{2F} (▲) at 25.2 MHz. Solid and dotted lines are the best-fitted calculated values. The broken lines show the phase transition temperatures determined by DSC.

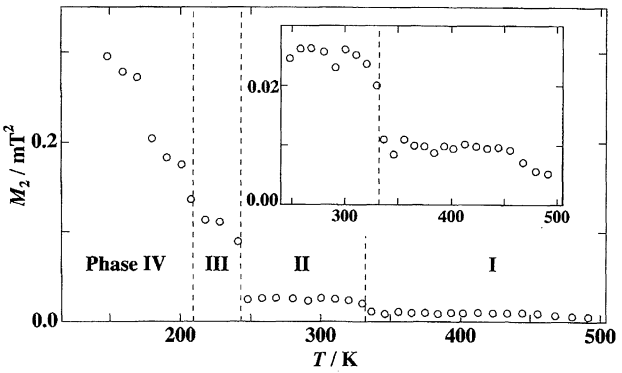

Fig. 9. The temperature dependence of second moment (M_2) of ^1H NMR linewidth observed in $[(CH_3)_3NC_2H_5]NO_3$. The broken lines show the phase transition temperatures determined by DSC.

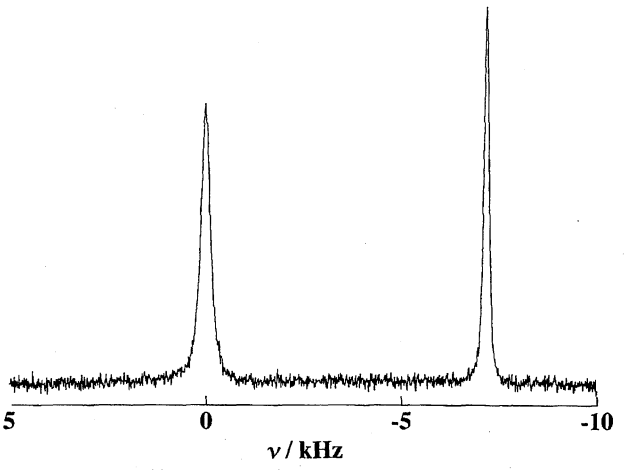

Fig. 10. The ^{14}N NMR spectrum observed at 340 K in Phase I of $[(CH_3)_3NC_2H_5]NO_3$.

at 26.9 MHz and T_2 of ^{19}F NMR (abbreviated to T_{2F}) at 25.2 MHz in Phases II and I. In Phase I, T_{1H} and T_{1F} showed a maximum and both T_{2H} and T_{2F} increased ca. 100 μs to 1 ms with increasing temperature from 420 to 510 K.

(3) $[(CH_3)_3NC_2H_5]NO_3$. The temperature dependence of M_{2H} observed at 49.1 MHz is shown in Fig. 9. M_{2H} was $(29.5\pm1.5)\times10^{-2}$ mT^2 at 155 K in Phase IV. With increasing temperature, M_{2H} decreased and reached almost constant values of $(2.5\pm0.2)\times10^{-2}$ and $(0.9\pm0.3)\times10^{-2}$ mT^2 in Phases II and I, respectively. The ^{14}N NMR spectrum observed at 340 K (Phase I) is shown in Fig. 10. The spectrum consisted of two liquid-like sharp lines. Since a 10% nitric acid was used for the reference, the peaks at −53 Hz ($\delta=-2.4$ ppm) and −7214 Hz ($\delta=-332.6$ ppm) were assigned to NO_3^- and $(CH_3)_3NC_2H_5^+$ ions, respectively. The data of T_{1H} determined at 49.1 and 19.2 MHz are shown in Fig. 11. Two T_{1H} minima were obtained around 140 K in Phase IV and around 250 K in Phase II for the resonance frequency of 49.1 MHz. An apparent discontinuity in T_{1H} was observed at each solid–solid phase transition point.

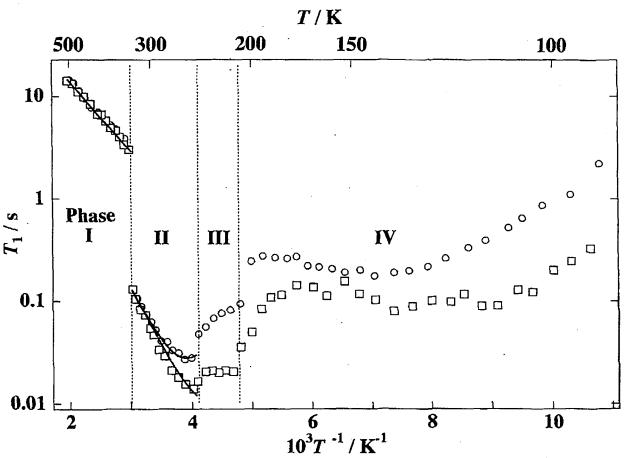

Fig. 11. The temperature dependence of ^1H NMR spin–lattice relaxation time (T_{1H}) observed in $[(CH_3)_3NC_2H_5]NO_3$. T_{1H} (○) observed at 49.1 MHz; T_{1H} (□) at 19.2 MHz. Solid lines are the best-fitted calculated values. The broken lines show the phase transition temperatures determined by DSC.

Discussion

Molecular Motions in Phases II and I of $[(CH_3)_3NC_2H_5]ClO_4$. In order to determine cationic motions occurring in Phase II, we compared the observed M_{2H} values with those calculated for various motional modes of the cation.[1,2] The intra-cationic contribution to M_{2H} from ^1H–^1H dipolar interactions was 1.1×10^{-2} mT^2 for the case that the cation performs the following three kinds of motions: the C_3 reorientation of all four CH_3 groups around the C–N or C–C bond axis, the C_3' reorientation of the whole $(CH_3)_3N$ group, and the rotation of the CH_3CH_2 group around the C–N bond axis. The last motion causes atomic disorder in the carbon position. The inter-ionic contribution to M_{2H} was not exactly evaluated because of the lack of detailed crystal data but was roughly estimated to be ca. 1×10^{-2} mT^2 on the basis of the crystal structure in the room temperature phase of $[(CH_3)_3NC_2H_5]I$.[1] When the cation performs the isotropic rotation, the intra-cationic contribution to M_{2H} vanishes and only the inter-ionic contribution remains. This contribution was calculated to be 0.64×10^{-2} mT^2 from the structure of Phase I. The value for the same motion in Phase II is expected to be larger, because Phase II is denser than Phase I and the averaged inter-cationic distance in Phase II is shorter than that in Phase I. Since the M_{2H} plateau obtained between 260 and 390 K in Phase II was $(1.4\pm0.3)\times10^{-2}$ mT^2, being smaller than 2.1×10^{-2} mT^2 calculated for the above three motions expected in the low temperature range of Phase II, the cationic motion is considered to be close to the isotropic rotation. In other words, we can expect that the cation acquired the most part of orientational freedom in Phase II. This is consistent with the DSC result that $\Delta_{tr}S$ of 42 J K^{-1} mol^{-1} at T_{tr}(III→II) is much larger than that of 1.0 J K^{-1} mol^{-1} at T_{tr}(II→I).

The ^{14}N NMR spectra in this temperature range shown in Fig. 2 were explainable in terms of the same cationic motion, i.e. the isotropic rotation. The finite quadrupole coupling constant (qcc) of 7—8 kHz obtained seems to be mostly associated with the tetragonal distortion[11] of the crystal lattice in Phase II. This value is comparable to 5.8 kHz reported for Phase II of $[(CH_3)_3NC_2H_5]BF_4$ with a tetragonal structure, where the quasi-isotropic rotation of cation was detected.[2]

The quadrupole coupling constant decreased above 380 K and became 0.8 kHz at 430 K in Phase II, consistent with the M_{2H} decrease above 380 K from 1.4×10^{-2} mT^2 to less than 0.05×10^{-2} mT^2. These facts indicate that the rotational motion of cation becomes completely isotropic, averaging out the quadrupole coupling as well as the intra-cationic dipole–dipole interaction. Furthermore, the extremely small M_{2H}, less than 0.05×10^{-2} mT^2, indicates the occurrence of translational self-diffusion of the cation in Phase II, because lower values than the M_{2H} value of 0.64×10^{-2} mT^2 calculated for the isotropically rotating cations can only be explained by the onset of the cationic self-diffusion. At the same time, the gradual decrease of qcc upon heating in Phase II seems to be attributed to the strongly temperature-dependent lattice parameters and the symmetry at the ^{14}N site becomes close to cubic with increasing temperature.

The temperature dependence of T_{1H} observed in Phase II shown in Fig. 4 can be explained by the BPP equation[12] expressed as

$$T_{1H}^{-1} = C\{\tau/(1+\omega^2\tau^2)+4\tau/(1+4\omega^2\tau^2)\}, \quad (2)$$

where C, ω, and τ are the motional constant, the Larmor frequency, and correlation time of the motion, respectively. In the limit of $\omega\tau\ll1$, we have

$$T_{1H}^{-1} = 5C\tau. \quad (3)$$

Here τ is written by the Arrhenius-type equation:

$$\tau = \tau_0 \exp(E_a/RT), \quad (4)$$

where E_a is the activation energy. Applying Eqs. 3 and 4, we obtained E_a of 25±2 kJ mol^{-1} for the cationic isotropic rotation from the slope of log T_{1H} vs. T^{-1} plots.

The M_{2H} less than 0.05×10^{-2} mT^2 observed in Phase I indicates that the cation performs self-diffusion as well as isotropic rotation. The frequency dependent T_{1H} observed in Phase I was analyzed by assuming the presence of two superimposed relaxation processes, given by

$$T_{1H}^{-1} = T_{1H,rot}^{-1} + T_{1H,dif}^{-1}. \quad (5)$$

Here, $T_{1H,rot}$ is the contribution from the cationic rotation whose correlation time τ_{rot} is expected to be short enough to satisfy the condition of $\omega\tau_{rot}\ll1$. $T_{1H,dif}$ arises from the cationic self-diffusion, which is assumed to be slow in this temperature range; i.e. the condition of $\omega\tau_{dif}\gg1$ is fulfilled, where τ_{dif} is the correlation time of cationic self-diffusion. Applying these two conditions for the two kinds of cationic motion to Eq. 2, we can rewrite Eq. 5 as

$$T_{1H}^{-1} = 5C_{rot}\tau_{rot} + 2C_{dif}\omega^{-2}\tau_{dif}^{-1}, \quad (6)$$

where C_{rot} and C_{dif} denote motional constants of the two cationic motions. Assuming the temperature dependence of both τ_{rot} and τ_{dif} to be Arrhenius-type as expressed by Eq. 4, we evaluated the activation energies for the cationic self-diffusion and isotropic rotation to be 60±2 and 27±3 kJ mol^{-1}, respectively.

The increase in T_2 from 80 to 800 μs above 400 K in Phase II and that from 1 to 15 ms in Phase I are attributed to cationic self-diffusion, because the onset of this motion was shown in the M_{2H} analysis given above. When T_{2H} can be expressed by the BPP-type equation under the condition of $\omega\tau_{dif}\gg1$, we have

$$T_{2H} \propto \tau_{dif}^{-1}. \quad (7)$$

The activation energies of cationic self-diffusion in Phases II and I were evaluated to be 117±5 and 60±2 kJ mol^{-1}, respectively, from the slope of the log T_{2H} vs. T^{-1} plots, by using Eqs. 4 and 7. The values obtained are summarized Table 6.

Molecular Motions in Phases II and I of $[(CH_3)_3NC_2H_5]PF_6$. The linewidth of 460—910 Hz of ^{14}N NMR spectra obtained in Phase II is comparable to that observed in the

Table 6. Activation Energies for Cationic and Anionic Motions in Phases I and II of $[(CH_3)_3NC_2H_5]X$ (X=ClO_4, PF_6, NO_3) Evaluated from ^1H and ^{19}F NMR Relaxation Data

Compound	E_a (kJ mol^{-1})	Method	Motional mode
$[(CH_3)_3NC_2H_5]ClO_4$			
Phase I	27±3	T_{1H}	Cationic isotropic rotation
	60±2	T_{1H}	Cationic self-diffusion
	60±2	T_{2H}	Cationic self-diffusion
Phase II	25±2	T_{1H}	Cationic isotropic rotation
	117±5	T_{2H}	Cationic self-diffusion
$[(CH_3)_3NC_2H_5]PF_6$			
Phase I	19±3	T_{1H}	Cationic isotropic rotation
	56±3	T_{1H}	Cationic self-diffusion
	59±4	T_{2H}	Cationic self-diffusion
	5±1	T_{1F}	Anionic isotropic rotation
	53±3	T_{1F}	Anionic self-diffusion
	53±3	T_{2F}	Anionic self-diffusion
Phase II	23±2	T_{1H}	Cationic isotropic rotation
	12±1	T_{1F}	Anionic isotropic rotation
$[(CH_3)_3NC_2H_5]NO_3$			
Phase I	13±1	T_{1H}	Cationic isotropic rotation
Phase II	22±1	T_{1H}	Rotation of CH_3CH_2 group

high-temperature region of Phase II of perchlorate. The intra-molecular ^{14}N quadrupole couplings are, therefore, considered to be averaged out by the cationic rotation, but there should be a contribution from the tetragonally distorted lattice which gave the observed linewidth. The shape of ^{14}N NMR spectra, which is a structureless single peak different from that observed in Phase II of perchlorate, may be explained by the large positional distribution of N atom around the centre of cationic rotation caused by various rotational modes of cations.

The spherical anion with a size smaller than that of the cation is also considered to perform the same motion from the fact that the constant M_{2F} value of 2.2×10^{-2} mT^2 observed in Phase II is comparable to the M_{2F} value of 1.9×10^{-2}—3.3×10^{-2} mT^2 obtained in NH_4PF_6, where the isotropic rotation of NH_4^+ and PF_6^- ions was reported.[13,14] The M_{2H} value of 1.5×10^{-2} mT^2 observed in Phase II is, therefore, attributable to the isotropic rotation of both cation and anion. The presence of isotropic rotation is supported by the very small $\Delta_{tr}S$ of 0.75 J K^{-1} mol^{-1} observed at T_{tr}(II→I), implying that orientational freedom of the ions in Phase II is nearly the same as that in Phase I, where isotropic rotation of both cation and anion were definitely revealed as shown below.

The cationic and anionic isotropic rotations are also considered to be mainly effective in T_{1H} and T_{1F} in Phase II, respectively, from the facts that T_{1H} and T_{1F} show exponential behaviour and the slopes of log T_{1H} vs. T^{-1} and log T_{1F} vs. T^{-1} are different as shown in Figs. 7 and 8. Applying Eqs. 3 and 4 to T_{1H} and T_{1F} data, we obtained E_a of 23±2 and 12±1 kJ mol^{-1} for the cationic and anionic isotropic rotation, respectively.

In Phase I, both M_{2H} and M_{2F} decreased to less than 0.05×10^{-2} mT^2 above 485 K. Since M_{2H} and M_{2F} for the isotropic rotation of cation and anion were calculated to be 0.77×10^{-2} and 0.77×10^{-2} mT^2, respectively, using the structural data in Phase I of $[(CH_3)_3NC_2H_5]PF_6$, the decrease in M_{2H} and M_{2F} is attributed to the onset of self-diffusion of both ions. The observed T_{1H} and T_{1F} having a maximum in Phase I were analysed by using Eqs. 4, 5, and 6, assuming that both isotropic rotation and self-diffusion in the cation and the anion mainly affect T_{1H} and T_{1F}, respectively. We have obtained E_a of 19±3 and 56±3 kJ mol^{-1} for the cationic isotropic rotation and self-diffusion, respectively, and 5±1 and 53±3 kJ mol^{-1} for the anionic isotropic rotation and self-diffusion. From the M_{2H} and M_{2F} results, the increase in T_{2H} and T_{2F} observed above 420 K is attributed to the cationic and anionic self-diffusion, respectively. We obtained E_a of 59±4 kJ mol^{-1} for the cation and 53±3 kJ mol^{-1} for the anion from the slope of the log T_{2H} vs. T^{-1} and the log T_{2F} vs. T^{-1} plots by using Eqs. 4 and 7.

Molecular Motions in Phases II and I of $[(CH_3)_3NC_2H_5]NO_3$. The constant M_{2H} value of 2.5×10^{-2} mT^2 observed in Phase II shown in Fig. 9 can be attributed to a composite cationic motion of the C_3 reorientation of all four CH_3 groups around the C–N or C–C bond axis, the C_3' reorientation of the whole $(CH_3)_3N$ group, and the rotation of the CH_3CH_2 group around the C–N bond axis, by referring to the M_{2H} value of ca. 2×10^{-2} mT^2 calculated for this mode of motions as discussed above. This phase is, therefore, a dynamically disordered phase concerning the orientation of the CH_3CH_2 group. Among these motions, the rotation of CH_3CH_2 group is considered to be the most hindered motion, i.e. the slowest motion, because this requires additional void space in the crystal, causing the dynamically disordered state of cation. The other motions are already excited in the low-temperature

phases as discussed below. We can, therefore, attribute the effective mechanism on T_{1H} observed in Phase II shown in Fig. 11 to the CH_3CH_2 group motion. Equations 2 and 4 were fitted to the T_{1H} data and E_a of 22±1 kJ mol^{-1} was obtained for this motion.

As shown in Fig. 10, the two sharp peaks in ^{14}N NMR obtained in Phase I, which are assigned to N atoms in the anion and the cation, indicate that both ions perform isotropic rotation. The rotation of the cation was also indicated by the M_{2H} value of 0.91×10^{-2} mT^2 obtained in Phase I, because this value is close to 0.80×10^{-2} mT^2 calculated for this motion from the structure of this phase. By fitting Eqs. 3 and 4 to the T_1 data in Phase I, we obtained E_a of 13±1 kJ mol^{-1} for this motion from the slope of log T_{1H} vs. T^{-1} plots.

The structure of Phase I is the NaCl-type cubic lattice; this is the same as that of Phase I of $[(CH_3)_3NC_2H_5]X$ (X = I, BF_4), in which the anionic self-diffusion was detected.[1,2] The effective radii of $[(CH_3)_3NC_3H_5]^+$ in Phases I of these three salts evaluated from the lattice constants were 3.08, 2.80, and 2.79 Å for nitrate, iodide and tetrafluoroborate, respectively, using the values of $r(NO_3^-)$ = 1.89 Å, $r(I^-)$ = 2.20 Å, and $r(BF_4^-)$ = 2.28 Å for the effective radii of the anions performing isotropic rotation.[15] These cationic radii imply that, among these three salts, nitrate has the largest void space in the crystal. This means the weakest interaction between anions and cations in nitrate, suggesting that the NO_3^- ion also can diffuse in Phase I of $[(CH_3)_3NC_2H_5]NO_3$.

Motions in Lower Temperature Phases of $[(CH_3)_3NC_2H_5]X$ (X=ClO_4, PF_6, NO_3). The constant M_{2H} value of $(17.8\pm0.5)\times10^{-2}$ mT^2 observed for $[(CH_3)_3NC_2H_5]ClO_4$ between 150 and 210 K shown in Fig. 1 is comparable to the calculated value of 18.6×10^{-2} mT^2 (intra-cationic and inter-ionic contributions to M_{2H} are 13.4×10^{-2} and 5.2×10^{-2} mT^2, respectively) for the C_3 reorientation of the three CH_3 groups in the $(CH_3)N$ group around the respective C–N bond axis, which value was evaluated by use of the structure in Phase III of $[(CH_3)_3NC_2H_5]I$.[1] The M_{2H} decreased above 210 K and reached to 8×10^{-2} mT^2 at 258 K in Phase III. This value is close to that of 7.0×10^{-2} mT^2 (intra-cation and inter-ionic contributions are 4.3×10^{-2} and 2.7×10^{-2} mT^2, respectively) for the C_3 reorientation of all four CH_3 groups in $(CH_3)_3N$ and CH_3CH_2 groups as well as the C_3' reorientation of the whole $(CH_3)_3N$ group.[1] We can, therefore, conclude that, in Phase III, the reorientations in three CH_3 groups are excited first at low temperatures and then the remaining CH_3 group and $(CH_3)_3N$ group motions are excited. From the M_{2H} results, the T_{1H} minimum observed at ca. 165 K in Phase III of $[(CH_3)_3NC_2H_5]ClO_4$ shown in Fig. 3 is attributable to the C_3 reorientation of three CH_3 groups in the cation, and the T_{1H} minimum at ca. 240 K to the C_3' reorientation of $(CH_3)_3N$ group and the C_3 reorientation of the rest CH_3 group.

The M_{2H} value of 42.1×10^{-2} mT^2 observed at 173 K in Phase IV of $[(CH_3)_3NC_2H_5]PF_6$ given in Fig. 5 is attributable to the rigid lattice, and the plateau values of 8.5×10^{-2} mT^2 in Phase III to the C_3 reorientation of all four CH_3 groups together with the C_3' reorientation of $(CH_3)_3N$ group. The deep T_1 minimum around 200 K shown in Fig. 7 is, therefore, assigned to the above composite motion of the cation. The M_{2F} values of $(3.0\pm1.0)\times10^{-2}$ and $(2.2\pm0.6)\times10^{-2}$ mT^2 observed in Phases IV and III, respectively, are attributable to the isotropic rotation of the anion by referring to the M_{2F} results obtained in NH_4PF_6.[13,14] The M_{2F} in Phase III smaller than in Phase IV is explainable by the difference in the contributions from the ^{19}F–^{1}H dipole interaction between the anion and cation in these two phases, because the cationic motions excited in Phase III partly average out the ^{19}F–^{1}H interaction. The two T_{1F} minima observed at 100 and 140 K, therefore, are assigned to this motion; the low and high temperature T_{1F} minima are considered to arise from ^{19}F–^{19}F and ^{19}F–^{1}H dipolar interactions, respectively.

The decrease in M_{2H} from 29.5×10^{-2} to 8×10^{-2} mT^2 with increasing temperature in Phases IV and III of $[(CH_3)_3NC_2H_5]NO_3$ shown in Fig. 9 implies that the C_3 reorientation of four CH_3 groups and the C_3' reorientation of $(CH_3)_3N$ group are excited in these phases. By referring to the M_{2H} results and the T_{1H} minimum values obtained in $[(CH_3)_3NC_2H_5]I$,[1] the T_{1H} minimum observed around 140 K at 49.1 MHz in Phase IV and the T_{1H} decrease in Phase III shown in Fig. 11 are attributable to one of four CH_3 groups and the other three CH_3 groups, respectively. The $(CH_3)_3N$ group motion in these phases is considered to be too slow to be detected by T_{1H}.

DSC and X-Ray Diffraction. As shown in Table 5, all of the highest-temperature solid phases of $[(CH_3)_3NC_2H_5]$-X (X=ClO_4, PF_6, NO_3, I, BF_4) are cubic, indicating that both cations and anions isotropically rotate satisfying the cubic symmetry. The radii of the anions performing isotropic rotation are in the order of $NO_3^- < I^- < BF_4^- < ClO_4^- < PF_6^-$.[15,16] The salts consisting of large anions of ClO_4^- and PF_6^- form the CsCl-type cubic lattice, while the others the NaCl-type. From the crystal structure and the ionic motions revealed, the cations and anions in Phase I are dynamically disordered around their centre of gravity and considered to obtain the greatest part of the motional freedom, i.e., orientational freedom and hence the entropy of fusion is expected very small. In fact, the value observed in iodide was only 5.5 J K^{-1} mol^{-1}, being much lower than 20 J K^{-1} mol^{-1}, accepted as the criterion for the formation of the plastic phase in molecular crystals.[5]

It is interesting to note that the sums of $\Delta_{tr}S$ observed between 150 K and the highest-temperature solid phase are 43, 53, and 40.0 J K^{-1} mol^{-1} for perchlorate, nitrate and iodide, respectively, while those for tetrafluoroborate and hexafluorophosphate are 27.8 and 12.8 J K^{-1} mol^{-1}, respectively. Since the disordered states of cations and anions in the highest-temperature phases of these five salts are close to each other, we can expect a value of 40—50 J K^{-1} mol^{-1} for the sum of $\Delta_{tr}S$ for tetrafluoroborate and hexafluorophosphate, assuming that the configurational entropy is the most dominant contribution to $\Delta_{tr}S$ as reported in various ionic solids.[17] The discrepancy between the observed and expected values may be explained by that the lowest temperature phases observed for tetrafluoroborate and hexafluorophosphate are still

a disordered state and that ordered phases of these salts thus exist at lower temperatures.

Concluding Remarks

We have revealed that the cations are dynamically disordered in the highest- and second highest-temperature solid phases (Phases I and II) of $[(CH_3)_3NC_2H_5]X$ (X=ClO_4, PF_6, NO_3). Phase I of these salts crystallizes in the cubic structure like the highest-temperature phases of $[(CH_3)_3NC_2H_5]X$ (X=I, BF_4).[1,2] The salts consisting of large anions (ClO_4^-, PF_6^-) form the CsCl-type cubic lattice, while those having small anions (NO_3^-, I^-, BF_4^-) the NaCl-type lattice. Isotropic rotations of both cation and anion were observed in both types of cubic phases. Self-diffusion of the bulky cation was detected only in the CsCl-type cubic phase, while that of the anions smaller in size is considered to be excited in both types of cubic phases. Since the dynamical behavior of the constituent ions in Phase I of perchlorate and hexafluorophosphate is quite analogous to that in the plastic phase found in various molecular crystals,[5] we can conclude that Phase I of the two salts is the ionic plastic phase. Such a phase has been recently shown to exist in various methyl-substituted ammonium,[18,19] guanidinium[20,21] and alkali metal salts.[22—24] Some differences in thermal behaviour such as the temperature range of Phase I were observed between perchlorate and hexafluorophosphate, both of which consist of a spherical monovalent anion. This difference seems to be attributed to the size ratio of the cation and anion. Analogous differences in these anions were observed in piperidinium and pyrrolidinium salts which will be reported shortly.

Phase II of perchlorate and hexafluorophosphate crystallizes in a tetragonal lattice where the isotropic rotation of both cation and anion was observed. Moreover, self-diffusion of the cation was detected in Phase II of perchlorate. From the NMR and DSC results, the ions in Phase II of these two salts are considered to be dynamically disordered as highly as in Phase I. On the other hand, only the disordering of CH_3CH_2 group of the cation was observed in Phase II of nitrate.

This work was partly supported by Grant-in Aid for Scientific Research No. (A) 08554027 and (B) 09440234 from the Ministry of Education, Science, Sports and Culture.

References

1) H. Ishida, Y. Furukawa, S. Kashino, S. Sato, and R. Ikeda, *Ber. Bunsenges. Phys. Chem.*, **100**, 433 (1996).
2) H. Ono, R. Ikeda, and H. Ishida, *Ber. Bunsenges. Phys. Chem.*, **100**, 1833 (1996).
3) H. Ono, R. Seki, R. Ikeda, and H. Ishida, *J. Mol. Struct.*, **345**, 235 (1995).
4) M. Tansho, Y. Furukawa, D. Nakamura, and R. Ikeda, *Ber. Bunsenges. Phys. Chem.*, **96**, 550 (1992).
5) "The Plastically Crystalline State," ed by J. N. Sherwood, Wiley, New York (1979).
6) J. M. Chezeau and J. H. Strange, *Phys. Rep.*, **53**, 1 (1979).
7) J. G. Powles and J. H. Strange, *Proc. Phys. Soc.*, **82**, 6 (1963).
8) T. Kobayashi, H. Ohki, and R. Ikeda, *Mol. Cryst. Liq. Cryst.*, **257**, 279 (1994).
9) E. L. Hahn, *Phys. Rev.*, **80**, 580 (1950).
10) J. H. Davis, K. R. Jeffrey, M. Bloom, and M. I. Valic, *Chem. Phys. Lett.*, **42**, 390 (1976).
11) T. K. Pratum and M. P. Klein, *J. Magn. Reson.*, **53**, 473 (1983).
12) A. Abragam, "The Principles of Nuclear Magnetism," Oxford University Press, London (1961).
13) S. Albert and H. S. Gutowsky, *J. Chem. Phys.*, **59**, 3585 (1973).
14) R. Kaliaperumal, R. Srinivasan, and K. V. Ramanathan, *Chem. Phys. Lett.*, **102**, 29 (1983).
15) A. F. Kapustinskii, *Q. Rev. Chem. Soc.*, **10**, 283 (1956).
16) H. Bode and H. Clausen, *Z. Anorg. Allge. Chem.*, **265**, 229 (1951).
17) N. G. Parsonage and L. A. K. Staveley, "Disorder in Crystals," Clarendon Press, Oxford (1978).
18) H. Ishida, N. Hayama, and R. Ikeda, *Chem.Lett.*, **1992**, 1333.
19) H. Ishida, T. Iwachido, and R. Ikeda, *Ber. Bunsenges. Phys. Chem.*, **96**, 1468 (1992), and references therein.
20) S. Gima, Y. Furukawa, and D. Nakamura, *Ber. Bunsenges. Phys. Chem.*, **88**, 939 (1984).
21) Y. Furukawa and R. Ikeda, *Ber. Bunsenges. Phys. Chem.*, **97**, 1143 (1993).
22) K. Moriya, T. Matsuo, and H. Suga, *Thermochim. Acta*, **132**, 133 (1988).
23) Y. Furukawa, *J. Mol. Struct.*, **345**, 119 (1995).
24) R. Ikeda, S. Ishimaru, T. Tanabe, and D. Nakamura, *J. Mol. Struct.*, **345**, 151 (1995).